Inorg. Chem. **2008**, *47*, 4696−4705

Distinct Reaction Pathways of Peralkylated $Ln^{II}Al^{III}$ Heterobimetallic Complexes with Substituted Phenols†

Hanne-Marthe Sommerfeldt, Christian Meermann, Karl W. Törnroos, and Reiner Anwander*

Department of Chemistry, University of Bergen, Allégaten 41, N-5007 Bergen, Norway

Received December 31, 2007

The protonolysis reaction of heterobimetallic peralkylated complexes $[Ln(AlR_4)_2]_n$ (Ln = Sm, Yb; R = Me, Et) with 2 equiv of $HOC_6H_2tBu_2$-2,6-Me-4 affords the bis(trialkylaluminum) adducts $Ln[(\mu\text{-}OAr^{tBu,Me})(\mu\text{-}R)AlR_2]_2$ in good yields. Analogous reactions with the less sterically demanding *i*Pr-substituted phenol result in ligand redistributions and formation of X-ray structurally evidenced $Ln[(\mu\text{-}OAr^{iPr,H})_2AlR_2]_2$ (Ln = Yb, R = Me; Ln = Sm, R = Et), $Yb[(\mu\text{-}OAr^{iPr,H})(\mu\text{-}Et)AlEt_2]_2(THF)$, and $[Et_2Al(\mu\text{-}OAr^{iPr,H})_2Yb(\mu\text{-}Et)_2AlEt_2]_2$. The solid-state structures of serendipitous alumoxane complex $Sm[(\mu\text{-}OAr^{tBu,Me})AlEt_2OAlEt_2(\mu\text{-}OAr^{tBu,Me})](toluene)$ and dimeric $AlMe_3$-adduct complex $[(AlMe_3)(\mu\text{-}OAr^{tBu,Me})Sm(\mu\text{-}OAr^{tBu,Me})_2Sm(\mu\text{-}OAr^{tBu,Me})(AlMe_3)]$ were also determined by X-ray crystallography. While the former can be discussed as a typical hydrolysis product of $Sm[(\mu\text{-}OAr^{tBu,Me})(\mu\text{-}Et)AlEt_2]_2$, the latter was isolated from the 1:1 reaction of $[Sm(AlEt_4)_2]_n$ with $HOAr^{tBu,Me}$.

Introduction

Aryloxide (phenolate) moieties $[OAr^R]$ provide versatile ancillary ligand sets for the highly oxophilic rare-earth metal centers and have been widely used as monovalent $[\mathbf{O}]^-$ and chelating divalent $[\mathbf{O}(Do)_n\mathbf{O}]^{2-}$ derivatives (Do = neutral donor functionalitiy, $n = 0, 1, 2$).[1,2] While the latter received considerable attention as stabilizing ligands in organolanthanide catalysis (e.g., linked bis(phenolates) or SALEN-type ligands),[3−12] the former promote valuable synthesis protocols aiming at metal alkylation.[13,14] Accordingly, the alkylation receptivity of homoleptic complexes $Ln(OAr^R)_3$ in the presence of organoaluminum compounds, in particular $[AlMe_3]$ (TMA) and $[AlEt_3]$ (TEA), has been studied in detail.[14] It was found that product formation in reaction mixtures $Ln(OAr^R)_3/[AlR_3]$ is mainly governed by the size of the rare-earth metal center and the substitution pattern of the aryloxide ligand. X-ray crystallographically authenticated alkylated $Ln^{III}-Al^{III}$ heterobimetallic complexes are depicted in Chart 1, showing organoaluminum adduct formation (**A**),[15−19] [phenolate] → [alkyl] interchange (**B**),[17] and ligand redistribution (**C**, **D**)[20,21] as the predominant reaction pathways.

Because the reaction outcome is decisively affected by the Ln^{III} cation size, different product spectra could be anticipated for similar transformations involving the larger

* To whom correspondence should be addressed. Fax: (+47) 5558-9490. Phone: (+47) 5558-9491. E-mail: reiner.anwander@kj.uib.no.

† Dedicated to Prof. Jon Songstad on the occasion of his 70th birthday.

(1) Anwander, R. *Top. Curr. Chem.* **1996**, *179*, 149.
(2) Bradley, D. C.; Mehrota, R. C.; Rothwell, I. P.; Singh, A. *Alkoxo and Aryloxo Derivatives of Metals*; Academic Press: San Diego, CA, 2001; p 704.
(3) Piers, W. E.; Emslie, D. J. H. *Coord. Chem. Rev.* **2002**, *233–234*, 131.
(4) Hou, Z.; Wakatsuki, Y. *Coord. Chem. Rev.* **2002**, *231*, 1.
(5) Cozzi, P. G. *Chem. Soc. Rev.* **2004**, *33*, 410.
(6) Aspinall, H. C. *Chem. Rev.* **2002**, *102*, 1807.
(7) Hultzsch, K. C. *Adv. Synth. Catal.* **2005**, *347*, 367.
(8) Hultzsch, K. C.; Gribkov, D. V.; Hampel, F. *J. Organomet. Chem.* **2005**, *690*, 4441.
(9) Larrow, J. F.; Jacobsen, E. N. *Top. Organomet. Chem.* **2004**, *6*, 123.
(10) Katsuki, T. *Chem. Soc. Rev.* **2004**, *33*, 437.
(11) Jacobsen, E. N. In *Catalytic Asymmetric Synthesis*; Ojima, I., Ed.; VCH: New York, 1993.
(12) Jacobsen, E. N. In *Comprehensive Organometallic Chemistry II*; Abel, E. W., Stone, F. G. A., Wilkinson, G., Hegedus, L. S., Eds.; Pergamon: Oxford, U.K., 1995; Vol. *12*.
(13) Anwander, R. *Top. Organomet. Chem.* **1999**, *2*, 1.
(14) Fischbach, A.; Anwander, R. *Adv. Polym. Sci.* **2006**, *204*, 155.
(15) Gordon, J. C.; Giesbrecht, G. R.; Brady, J. T.; Clark, D. L.; Keogh, D. W.; Scott, B. L.; Watkin, J. G. *Organometallics* **2002**, *21*, 127.
(16) Giesbrecht, G. R.; Gordon, J. C.; Brady, J. T.; Clark, D. L.; Keogh, D. W.; Michalczyk, R.; Scott, B. L.; Watkin, J. G. *Eur. J. Inorg. Chem.* **2002**, 723.
(17) Fischbach, A.; Herdtweck, E.; Anwander, R.; Eickerling, G.; Scherer, W. *Organometallics* **2003**, *22*, 499.
(18) Fischbach, A.; Meermann, C.; Eickerling, G.; Scherer, W.; Anwander, R. *Macromolecules* **2006**, *39*, 6811.
(19) Fischbach, A. PhD Thesis, Technische Universität München: München, Germany, 2003.
(20) Evans, W. J.; Ansari, M. A.; Ziller, J. W. *Inorg. Chem.* **1995**, *34*, 3079.
(21) Evans, W. J.; Ansari, M. A.; Ziller, J. W. *Polyhedron* **1997**, *16*, 3429.

10.1021/ic702517s CCC: $40.75
Published on Web 04/29/2008

Chart 1. X-ray Crystallographically Characterized Alkylated $Ln^{III}-Al^{III}$ Heterobimetallic Aryloxides

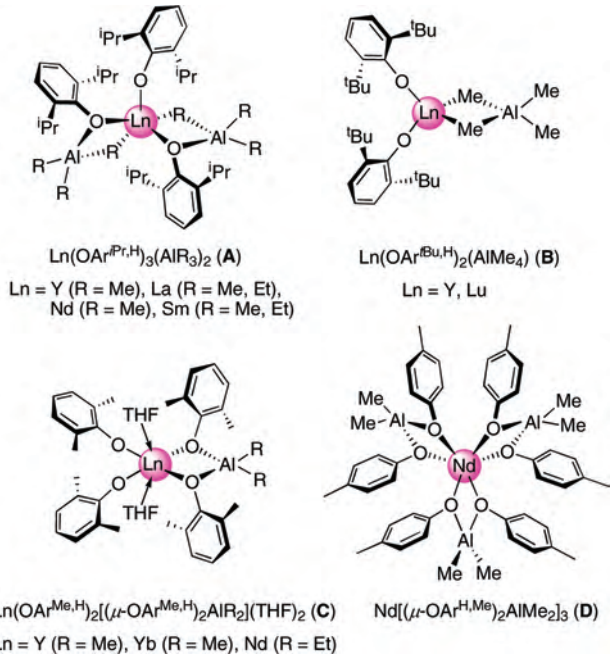

Scheme 1. TMA Adduct Formation versus Peralkylation of Lanthanide(II) Aryloxides with Excess of Trimethylaluminum[17]

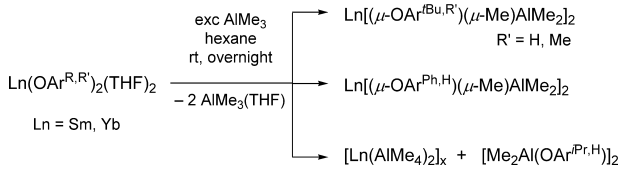

Ln^{II} metal centers. Herein we describe the synthesis and structural characterization of such alkylated Ln^{II}–Al^{III} heterobimetallic aryloxide complexes.

Results and Discussion

We have previously reported that TMA adduct formation and [phenolate] → [alkyl] interchange are the predominant reaction pathways when $Ln^{II}(OAr^R)_2(THF)_x$ are treated with TMA. As shown for a series of 2,6-di-*tert*-butyl- and diphenyl-substituted phenolate complexes of the divalent lanthanide metal centers samarium and ytterbium, homoleptic bis(trialkylaluminum) adducts $Ln[(\mu\text{-}OAr^R)(\mu\text{-}R)AlR_2]_2$ could be generated in good yields (Scheme 1).[17] Depending on the type of phenolate substituent in the 4-position (H vs Me vs *t*Bu) varying amounts of permethylated $[Ln(AlMe_4)_2]_x$ were obtained as byproducts. The sterically less crowded 2,6-iPr$_2$-substituted phenolates afforded homoleptic tetramethylaluminates in quantitative yields.[17] Unfortunately, such binary $Ln(OAr^R)_2(THF)_x/[AlR_3]$ mixtures did not afford single-crystalline mixed alkyl/aryloxide complexes.

The aim of the present study was therefore to apply a different reaction protocol. Peralkylated $[Ln(AlR_4)_2]_n$ (R = Me (**1**), Et (**2**); Ln = Sm (**a**), Yb (**b**)) are readily available $Ln^{II}-Al^{III}$ heterobimetallic complexes which were found to engage in protonolysis reactions with HC_5Me_5.[22] Aiming at bis(aryloxide) complexes $Ln^{II}[(OAr^R)_x(AlR_y)_z]$ of the **A**- and **B**-type (Chart 1), we examined the two equivalent reactions of complexes **1** (in toluene) and **2** (in hexane) with bulky 2,6-di-*tert*-butyl-4-methylphenol ($HOAr^{tBu,Me}$) and 2,6-di-isopropylphenol ($HOAr^{iPr,H}$) at ambient temperature (Scheme 2).

Protonolysis reactions occurred instantly as indicated by gas evolution and color change. The reaction mixtures were stirred overnight, filtered to remove possible insoluble starting materials, and the solvent evaporated. The obtained residues were examined by NMR spectroscopy either directly or after crystallization. The $Ln^{II}-Al^{III}$ heterobimetallic aryloxide complexes **3**−**10** could be isolated as dark-red (Sm) or yellow crystalline solids (Yb). Generally, the reactions gave complicated product mixtures containing up to three alkylation products. As a rule, fractionate crystallization was the only proper means to unequivocally characterize the reaction products. Single-crystal X-ray diffraction analyses were performed on complexes **4a**, **5**, **6**, **7b**, **8a**, **9**, and **10** after recrystallization from toluene or hexane at −35 °C. The fully characterized reaction products are shown in Scheme 2.

$[Ln(AlMe_4)_2]_n-HOAr^{tBu,Me}$ Reactions. Treatment of a suspension of $[Ln(AlMe_4)_2]_n$ in toluene with $HOAr^{tBu,Me}$ gave reddish brown (Ln = Sm, **3a**) or yellow (Ln = Yb, **3b**) compounds which could be crystallized from toluene in moderate yields. The ^{1}H NMR spectra of compounds **3** proved the formation of bis(TMA) adducts of the composition $Ln[(\mu\text{-}OAr^{tBu,Me})(\mu\text{-}Me)AlMe_2]_2$, in agreement with our previous findings using Ln^{II} aryloxides and excess $[AlMe_3]$ (Scheme 1).[17] Hence, the bis(TMA) adducts can be obtained by at least two different synthesis approaches. Unfortunately, single-crystals of **3b** from this alternative synthesis protocol provided only nonconclusive crystallographic data. In an attempt to access putative mono(TMA) adduct−tetramethylaluminate intermediates $Sm[(\mu\text{-}OAr^{tBu,Me})(\mu\text{-}Me)AlMe_2](AlMe_4)$, we reacted $[Sm(AlMe_4)_2]_n$ (**1a**) with only 1 equiv of $HOAr^{tBu,Me}$. However, unreacted **1a**, which was separated from the reaction mixture after 16 h of stirring at ambient temperature, pointed to a more complex protonolysis reaction. The toluene-soluble part of the reaction mixture was stored at −35 °C, and few single-crystals could be harvested after several months. X-ray diffraction analysis revealed the formation of complex $[AlMe_3(\mu\text{-}OAr^{tBu,Me})]Sm(\mu\text{-}OAr^{tBu,Me})_2Sm[(\mu\text{-}OAr^{tBu,Me})AlMe_3]$ (**5**, Figure 1, Table 1).

Complex **5** is in accordance with the initial occurrence of an extensive protonolysis reaction, with full $[AlMe_4]/[\mu\text{-}OAr^{tBu,Me}]$ ligand exchange. One can speculate about that the "relatively small" amount of TMA released by this one equivalent reaction might not be sufficient to completely disrupt the dimeric/oligomeric arrangement of $[Sm(OAr^{tBu,Me})_2]_n$. Such a scenario would make mono(TMA) adduct complex **5** a plausible intermediate in binary $Ln(OAr^{tBu,H})_2(THF)_x$/exc AlR_3 mixtures leading to the bis(TMA) adducts (Scheme 1). Alternatively,

(22) Sommerfeldt, H. M.; Meermann, C.; Schrems, M. G.; Törnroos, K. W.; Frøystein, N. Å.; Miller, R. J.; Scheidt, E.-W.; Scherer, W.; Anwander, R. **2008**, 1899.

Scheme 2. Reactivity of $[Ln(AlR_4)_2]_n$ (R = Me (**1**), Et (**2**); Ln = Sm (**a**), Yb (**b**)) toward bulky phenols $HOAr^{iPr,H}$ and $HOAr^{tBu,Me}$ [a]

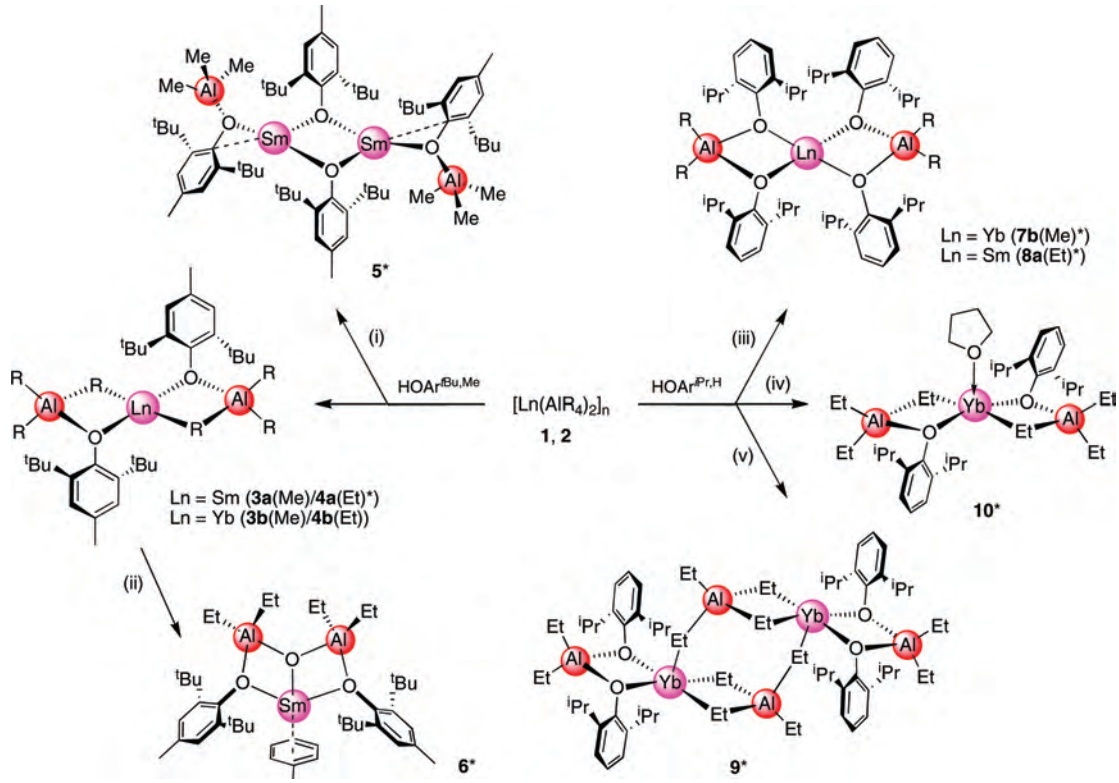

[a] All reactions were performed in toluene (for **1**) or hexane (for **2**) with 2 equiv of $HOAr^R$. Isolated complexes are shown only, and X-ray crystallographically authenticated complexes are denoted by asterisks. (i) Reaction performed in toluene with 1 equiv $HOAr^{tBu,Me}$. (ii) Degradation product, most likely the result of the presence of traces of H_2O. (iii) **7b** was also obtained with 4 equiv of $HOAr^{iPr,H}$. (iv) Coordinated THF possibly originates from $Yb(AlEt_4)_2(THF)_2$ present as a minor impurity. (v) Main product, but slower crystallization.

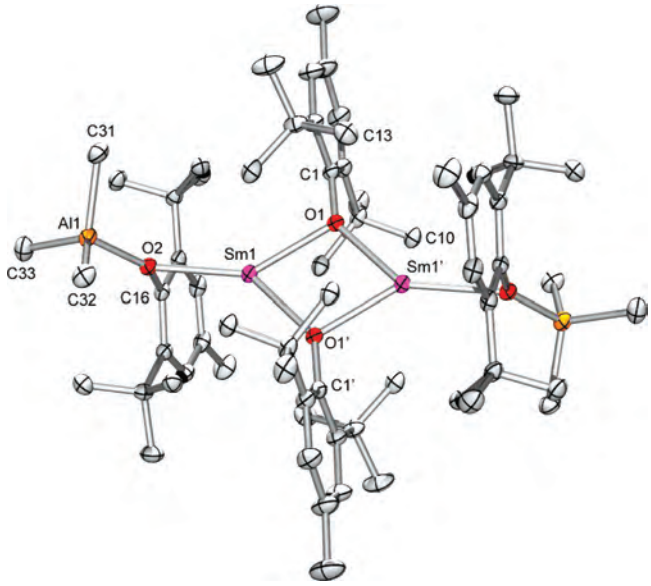

Figure 1. Molecular structure of **5** with atomic displacement parameters set at the 50% probability level. Hydrogen atoms are omitted for clarity.

Table 1. Selected Interatomic Distances (Å) and Angles (deg) for **5**

	bond distances		
Sm1···Sm1′	4.0036(2)	Al1−O2	1.8682(13)
Sm1−O1	2.4017(12)	O1−C1	1.365(2)
Sm1′−O1	2.4748(13)	O2−C16	1.369(2)
Sm1−O2	2.5953(12)	Al1−C31	1.992(2)
Sm1−C10′	3.142	Al1−C32	1.990(2)
Sm1−C13′	3.133	Al1−C33	1.993(2)
Sm1···C16	2.8412(17)		
	bond distances		
Sm1−O1−Sm1′	110.36(5)	Al1−O2−C16	140.41(11)
Sm1−O1−C1	140.33(11)	O1−Sm1−O1′	69.64(5)
Sm1′−O1−C1	109.07(10)	O1−Sm1−O2	141.17(4)
Sm1−O2−C16	85.66(9)	O2−Sm1−O1′	147.33(4)
Sm1−O2−Al1	133.93(6)		

extensive ligand redistribution could lead to the formation of compound **5**.

The molecular structure of **5** is comparable to dimeric $[Yb(OAr^{tBu,H})(\mu\text{-}OAr^{tBu,H})]_2$[23] (Table 2) except that the oxygen atoms of the terminal aryloxide each feature one coordinated TMA molecule. Such single mono[aryl(alk)oxide] bridges were previously observed in the only other reported Ln^{II}–Al^{III} heterobimetallic alkoxide complex, $[AlMe_3(\mu\text{-}OCH_2CH_2OMe)]Eu[(\mu\text{-}OCH_2CH_2OMe)_2AlMe_2]_2Eu[(\mu\text{-}OCH_2CH_2OMe)AlMe_3]$ (formula **E**, Chart 2).[24,25]

Another interesting structural feature of **5** is a rather acute Sm1−O2−C16 angle (85.66(9)°) and concomitant short contact of 2.8412(17) Å between the metal center and the *ipso*-carbon of the aromatic ring. This Sm1···C16 distance lies in the range of ordinary Sm^{II}−C bond lengths as reported for $[Sm\{C(SiMe_3)_2(SiMe_2OMe)\}_2(THF)]$ (2.787(5) and 2.845(5) Å)[26] and $Sm(AlEt_4)_2(THF)_2$ (2.774 Å).[27] Similar Ln−heteroatom−C_{ipso} bonding patterns were observed in $[\{[(Me_3Si)_2CH](C_6H_4\text{-}2\text{-}CH_2NMe_2)P\}_2Sm(THF)]$ (Sm···C =

(23) van den Hende, J. R.; Hitchcock, P. B.; Holmes, S. A.; Lappert, M. F. *J. Chem. Soc., Dalton Trans.* **1995**, 1435.

Table 2. Ln−O Bond Distances in Homoleptic and Heteroleptic Yb(II) and Sm(II) Aryloxides

compound[a]	Ln−O (Å)	Ln−(μ-O) (Å)	ref
homoleptic (+ donor)			
$[Yb(\mu\text{-}OC_6H_2tBu_2\text{-}2,6\text{-}Me\text{-}4)(OC_6H_2tBu_2\text{-}2,6\text{-}Me\text{-}4)]_2$	2.08(2), 2.10(2)	2.25(2)−2.37(2)	23, 31
$Yb(OC_6H_2tBu_2\text{-}2,6\text{-}Me\text{-}4)_2(L)_x$ (L = HMPA, THF, OEt_2)	2.126(9)−2.298(7)		32, 33
$[Yb(OC_6H_2tBu_3\text{-}2,4,6)_2(THF)_3](THF)_n$ (n = 0, 0.5)	2.219(8)−2.232(8)		34, 35
$Yb(OC_6H_3tBu_2\text{-}2,6)_2(NCMe)_4$	2.204(12), 2.245(10)		36
$[Yb(OC_6H_2tBu_2\text{-}2,6\text{-}OMe\text{-}4)_2(THF)_3](THF)$	2.229(5), 2.232(5)		37
$[Sm(OC_6H_2tBu_2\text{-}2,6\text{-}OMe\text{-}4)_2(THF)_3](THF)$	2.299(7), 2.305(7)		37
$[Sm(OC_6H_2tBu_2\text{-}2,6\text{-}Me\text{-}4)_2(THF)_3](L)$ (L = THF or MePh)	2.290(9)−2.347(13)		38–40
$[Sm(OC_6H_2tBu_3\text{-}2,4,6)_2(THF)_3](THF)$	2.325(6), 2.343(6)		41
$[KSm(OC_6H_2tBu_2\text{-}2,6\text{-}Me\text{-}4)_3(THF)]_\infty$	2.336(7)	2.362(6), 2.319(9)	42
heteroleptic			
$\{Yb(OC_6H_2tBu_2\text{-}2,6\text{-}Me\text{-}4)[(DIPPh)_2nacnac](THF)\}(THF)$	2.179(3)		43
$[Sm(OC_6H_2tBu_2\text{-}2,6\text{-}Me\text{-}4)(\mu\text{-}I)(THF)_3]_2(THF)_2$	2.300(10)		38
$(C_5Me_5)Sm(OC_6H_2tBu_2\text{-}2,6\text{-}Me\text{-}4)(HMPA)_2$	2.345(4)		38
$[(C_5Me_5)Sm(\mu\text{-}OC_6H_2tBu_3\text{-}2,4,6)]_2$		2.425(5),2.512(16)	30
$[(C_5Me_5)Sm(OC_6H_2tBu_2\text{-}2,6\text{-}R\text{-}4)(\mu\text{-}C_5Me_5)K(THF)_2]_\infty$ (R = H, Me)	2.29(2), 2.330(6)		30, 44

[a] [(DIPPh)$_2$nacnac] = Diisopropylphenyl β-diketiminate.

3.030(3) Å, Sm−P−C = 70.89(8)°),[28] and $[\{Me_2Al(\mu\text{-}Me_2)\}_2Nd(\mu_3\text{-}NPh)(\mu\text{-}Me)AlMe]_2$ (Nd···C = 2.723(6) Å, Nd−N−C = 87.03(3)°).[29] The Sm−C_{ipso} interactions in **5** imply longer Sm−O2 bond distances (2.5953(12) Å) than those of the asymmetrically homometal-bridging unit (2.4017(12) and 2.4748(13) Å). The latter Sm−O1/O1′ bond lengths, however, are similar to the ones reported for $[(C_5Me_5)Sm(\mu\text{-}OC_6H_2tBu_3\text{-}2,4,6)]_2$ (see Table 2).[30]

$[Ln(AlEt_4)_2]_n$−$HOAr^{tBu,Me}$ Reactions. Similar to the $[Ln(AlMe_4)_2]_n$-reactions, treatment of the perethylated complexes $[Ln(AlEt_4)_2]_n$ with two equivalents $HOAr^{tBu,Me}$ afforded reddish brown (Ln = Sm, **4a**) and yellow (Ln = Yb, **4b**) solids. The solution ^{1}H NMR spectra of **4** were consistent with the formation of bis(TEA) adducts $Ln[(\mu\text{-}OAr^{tBu,Me})(\mu\text{-}Et)AlEt_2]_2$. Dark-red single crystals of **4a** suitable for an X-ray structure analysis were grown from a hexane solution. Although low-quality crystallographic data unambiguously revealed the connectivity of **4a** as a bis(TEA) adduct, a detailed analysis of the metrical parameters is not warranted (Figure 2). The samarium atom is surrounded by two [(μ-Et)($AlEt_2$)] units and two aryloxide ligands, which are tilted toward the lanthanide center, resulting in short Sm−C_{ipso} contacts as observed in complex **5** (vide supra).

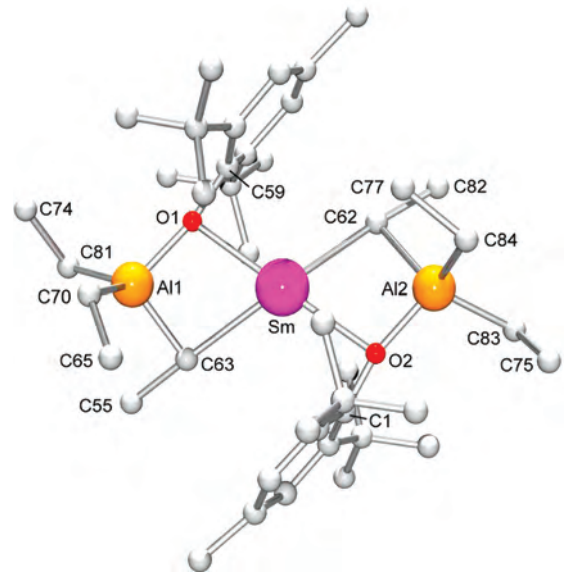

Figure 2. Ball and stick structure of **4a**.

Exhaustive recrystallization of compound **4a** from toluene yielded few dark-red single-crystals of plate-like morphology. The X-ray structure analysis revealed the formation of complex $Sm[(\mu\text{-}OAr^{tBu,Me})AlEt_2OAlEt_2(\mu\text{-}OAr^{tBu,Me})](toluene)$ (**6**) (Figure 3, Table 3), apparently generated by adventitious hydrolysis of **4a**. Thus, release of two ethane molecules and a concomitant alumoxane linkage accomplished a new tridentate bis(aryloxide)alumoxane ligand. The formation of the latter $[\mathbf{OOO}]^{2-}$–type ligand can also be rationalized by the templating action of the large Sm^{II} center. Complex **6** in a way provides additional evidence of the existence of bis(TEA) adducts **4**. Similar ethylalumoxane

(24) Evans, W. J.; Greci, M. A.; Ziller, J. W. *Inorg. Chem.* **1998**, *37*, 5221.
(25) For similar coordination motifs in alkaline earth metal chemistry, see: (a) Urko, J.; Szafert, S.; Jerzykiewicz, L. B.; Sobota, P. *Inorg. Chem.* **2005**, *44*, 5194. (b) Urko, J.; Ejfler, J.; Szafert, S.; John, L.; Jerzykiewicz, L. B.; Sobota, P. *Inorg. Chem.* **2006**, *45*, 5302.
(26) Clegg, W.; Eaborn, C.; Izod, K.; O'Shaughnessy, P.; Smith, J. D. *Angew. Chem., Int. Ed.* **1997**, *36*, 2815.
(27) Schrems, M. G.; Dietrich, H. M.; Törnroos, K. W.; Anwander, R. *Chem. Commun.* **2005**, 5922.
(28) Izod, K.; O'Shaughnessy, P.; Sheffield, J.; Clegg, W.; Liddle, S. *Inorg. Chem.* **2000**, *39*, 4741.
(29) Evans, W. J.; Ansari, M. A.; Ziller, J. W.; Khan, S. I. *Inorg. Chem.* **1996**, *35*, 5435.
(30) Hou, Z.; Zhang, Y.; Yoshimura, T.; Wakatsuki, Y. *Organometallics* **1997**, *16*, 2963.
(31) van den Hende, J. R.; Hitchcock, P. B.; Lappert, M. F. *J. Chem. Soc., Chem. Commun.* **1994**, 1413.
(32) Hou, Z. M.; Yamazaki, H.; Kobayashi, K.; Fujiwara, Y.; Taniguchi, H. *J. Chem. Soc., Chem. Commun.* **1992**, 722.
(33) Deacon, G. B.; Hitchcock, P. B.; Holmes, S. A.; Lappert, M. F.; Mackinnon, P.; Newnham, R. H. *J. Chem. Soc., Chem. Commun.* **1989**, 935.
(34) Trifonov, A. A.; Kirillov, E. N.; Fedorova, E. A.; Makarenko, N. P.; Bochkarev, M. N.; Schumann, H.; Muehle, S. *Russ. Chem. Bull.* **1998**, *47*, 2274.
(35) Deacon, G. B.; Feng, T.; Mackinnon, P.; Newnham, R. H.; Nickel, S.; Skelton, B. W.; White, A. H. *Aust. J. Chem.* **1993**, *46*, 387.
(36) Carretas, J.; Branco, J.; Marcalo, J.; Domingos, A.; Pires de Matos, A. *Polyhedron* **2003**, *22*, 1425.
(37) Deacon, G. B.; Fallon, G. D.; Forsyth, C. M.; Harris, S. C.; Junk, P. C.; Skelton, B. W.; White, A. H. *Dalton Trans.* **2006**, 802.
(38) Hou, Z.; Fujita, A.; Yoshimura, T.; Jesorka, A.; Zhang, Y.; Yamazaki, H.; Wakatsuki, Y. *Inorg. Chem.* **1996**, *35*, 7190.
(39) Qi, G. Z.; Shen, Q.; Lin, Y. H. *Acta Crystallogr., Sect. C* **1994**, *50*, 145.
(40) Yao, Y.-M.; Shen, Q.; Zhang, Y.; Xue, M.-Q.; Sun, J. *Polyhedron* **2001**, *20*, 3201.

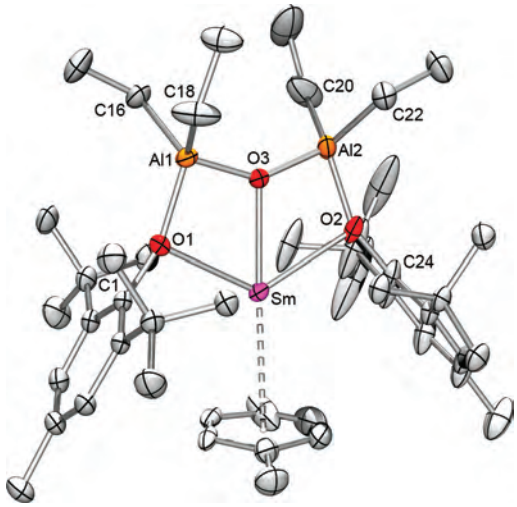

Figure 3. Molecular structure of **6** with atomic displacement parameters set at the 50% probability level. Hydrogen atoms and a second noncoordinating toluene molecule are omitted for clarity.

Table 3. Selected Interatomic Distances (Å) and Angles (deg) for **6**

	bond distances		
Sm···Al1	3.3320(7)	Al2−O2	1.857(2)
Sm···Al2	3.3314(8)	Al1−O3	1.7571(2)
Sm−O1	2.5525(17)	Al2−O3	1.7638(2)
Sm−O2	2.5522(18)	Al1−C16	1.987(3)
Sm−O3	2.3485(17)	Al1−C18	1.988(4)
Sm···C1	3.134(2)	Al2−C20	1.990(4)
Sm···C24	3.205(2)	Al2−C22	1.980(3)
Sm···Cnt[a]	2.935(7)	O1−C1	1.369(3)
Al1−O1	1.8518(18)	O2−C24	1.368(3)
	bond angles		
O1−Sm−O2	127.46(6)	Sm−O1−Al1	97.04(7)
Sm−O1−C1	101.84(13)	Sm−O2−Al2	96.89(7)
Sm−O2−C24	105.68(16)	Al1−O3−Al2	144.73(11)

[a] Cnt = ring centroid of the coordinated toluene molecule.

Chart 2. Unusual Al−O Interactions in Ln−Al^{III} Heterobimetallic Complexes

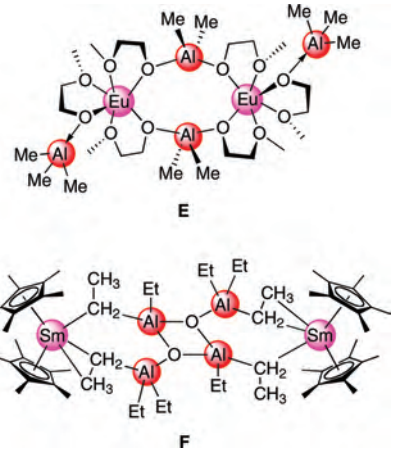

units have been found recently in a samarocene(III) complex **F** (Chart 2), obtained by treatment of carboxylate complex $[(C_5Me_5)_2Sm(\mu\text{-}O_2CPh)]_2$ with TEA.[45]

Coordination of the tridentate bis(aryloxide)alumoxane ligand renders the Sm^{II} center in complex **6** sterically unsaturated. The Sm−O−C_{ipso} angles of 101.84(13)° and 105.68(16)° are considerably less acute than in complex **5** (85.66(9)°); however, additional Sm···C_{ipso} contacts of av 3.170 Å seem to increase the coordination number. Moreover, a toluene molecule was found in close proximity to the Sm^{II} center, apparently residing in a coordination pocket formed by equidirectional tilting of the phenyl rings (cf., metal calix[*n*]arene complexes).[46,47] Significant π-coordination is indeed indicated by an average Sm−C(toluene) distance of 3.24 Å (Sm−Cnt = 2.935(7) Å). For comparison, the formally nine-coordinated (η^6-arene)Sm^{III}($AlCl_4$)$_3$ compounds show Sm−C(arene) bond distances in the range of 2.89 – 2.91 Å.[48] The Sm−O(aryloxide) bond lengths of av 2.552 Å are in the same range as found for **5**. The Sm−O(alumoxane) bond distance of 2.346(2) Å is the shortest Sm−[**OOO**] contact in **6** and is comparable to terminal Sm−O(aryloxide) bonds (Table 2).

[Ln(AlMe$_4$)$_2$]$_n$–HOAr^{iPr,H} Reactions. In contrast to the aforementioned HOAr^{tBu,Me} reactions, the less bulky phenol HOAr^{iPr,H} led to extensive ligand rearrangement at the large Ln^{II} metal centers (Scheme 2). Formation of large quantities of [$R_2Al(\mu\text{-}OAr^{iPr,H})]_2$,[49] which reassociate with the Ln^{II} metal centers to form bidentate ligands [$R_2Al(\mu\text{-}OAr^{iPr,H})_2$] is proposed. Such ligand rearrangement reactions are also common for Ln^{III} metal centers; however, in the presence of the smaller aryl(alk)oxide ligands [O*i*Pr],[50] [O*t*Bu],[51] [OAr^{Me,H}] (**C**),[20] and [OAr^{H,Me}] (**D**).[21,52] Complexes showing Ln^{III}[$R_2Al(\mu\text{-}OAr^{iPr,H})_2$] moieties, have not yet been reported. Note that Eu^{II} complex **E** (Chart 2) features bridging [$R_2Al(\mu\text{-}OR)_2$] ligands derived from the donor-functionalized ligand [OCH_2CH_2OMe].[24]

Instant reaction of [Ln(AlMe$_4$)$_2$]$_n$ (**1**) with 2 equiv of HOAr^{iPr,H} was indicated by gas evolution and color change of the reaction mixture. For ytterbium (**1b**), the pale yellow suspension turned into a red solution. The rearrangement product Yb[(μ-OAr^{iPr,H})$_2$AlMe$_2$]$_2$ (**7b**) was obtained in form of yellow crystals (45% yield). Surprisingly, unreacted or ligand-reassembled, toluene-insoluble starting material [Yb(AlMe$_4$)$_2$]$_n$ was not observed. At this place, one might have speculated about the formation of toluene-soluble π-coordinated coproducts Yb(AlMe$_4$)$_2$(C_6H_5Me), formed via protonolytic degradation of the polymeric network of **1b** and subsequent ligand rearrangement. For comparison, tetra-

(41) Yuan, F. G.; Zhu, X. H.; Weng, L. H. *Chinese J. Struct. Chem.* **2005**, *24*, 1152.
(42) Evans, W. J.; Anwander, R.; Ansari, M. A.; Ziller, J. W. *Inorg. Chem.* **1995**, *34*, 5.
(43) Yao, Y.; Zhang, Y.; Zhang, Z.; Shen, Q.; Yu, K. *Organometallics* **2003**, *22*, 2876.
(44) Hou, Z.; Zhang, Y.; Tezuka, H.; Xie, P.; Tardif, O.; Koizumi, T. A.; Yamazaki, H.; Wakatsuki, Y. *J. Am. Chem. Soc.* **2000**, *122*, 10533.
(45) Evans, W. J.; Champagne, T. M.; Ziller, J. W. *Organometallics* **2005**, *24*, 4882.
(46) Gutsche, C. D. *Calixarenes*; Royal Society of Chemistry: Cambridge, U.K., 1989.
(47) Asfari, Z.; Böhmer, V.; Harrowfield, J.; Vicens, J. *Calixarenes 2001*; Kluwer Academic: New York, 2001.
(48) Deacon, G. B.; Shen, Q. *J. Organomet. Chem.* **1996**, *506*, 1.
(49) Firth, A. V.; Stewart, J. C.; Hoskin, A. J.; Stephan, D. W. *J. Organomet. Chem.* **1999**, *591*, 185.
(50) Giesbrecht, G. R.; Gordon, J. C.; Clark, D. L.; Scott, B. L.; Watkin, J. G.; Young, K. J. *Inorg. Chem.* **2002**, *41*, 6372.
(51) Evans, W. J.; Boyle, T. J.; Ziller, J. W. *J. Am. Chem. Soc.* **1993**, *115*, 5084.
(52) Fischbach, A.; Perdih, F.; Herdtweck, E.; Anwander, R. *Organometallics* **2006**, *25*, 1626.

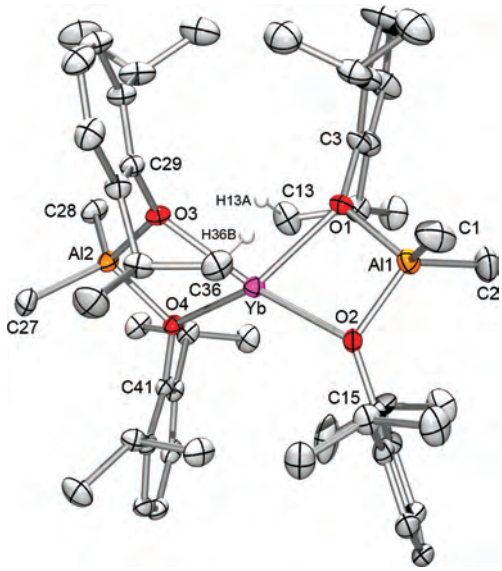

Figure 4. Molecular structure of **7b**. Atomic displacement parameters are set at the 50% probability level and hydrogen atoms are omitted for clarity, except for agostically interacting H36B and H13A.

chloro-aluminate complexes $[Yb(AlCl_4)_2]$ form soluble π-coordinated benzene and mesitylene derivatives.[53] However, the formation of π-coordinated coproducts $Yb(AlMe_4)_2(C_6H_5Me)$ can be ruled out on the basis of the NMR spectra, and unfortunately, we could not identify any other Yb^{II} reaction product. Complex **7b** was obtained in high yields by reaction of **1b** with 4 equiv of the phenol. In contrast, such rearrangement products were not observed when $Yb(OAr^{iPr,H})_2(THF)_2$ was treated with 6 equiv of TMA (cf., Scheme 1).[17] According to the ^1H NMR spectrum the corresponding samarium-reaction did also form one major product that we assign to $Sm[(\mu\text{-}OAr^{iPr,H})_2AlMe_2]_2$ (**7a**).

The molecular structure and metrical parameters of **7b** are shown in Figure 4 and Table 4, respectively. The ytterbium metal center adopts a distorted tetrahedral geometry. The average Yb−O distance of 2.384 Å lies somewhat above the expected range (cf., Table 2).

All the hydrogen atoms on the carbon atoms C13 and C36 were located in the difference Fourier maps and refined isotropically, indicating that the coordination sphere of the ytterbium center is additionally saturated by agostic interactions with two of the *i*Pr groups, resulting in short Yb···C and Yb···H distances (Yb···C13 = 3.055(4) Å, Yb···H13A = 2.56(3) Å, Yb···C36 = 3.067(4) Å, Yb···H36B = 2.52(3) Å). The average Al−O bond distance (1.839 Å), O−Yb−O bond angle (66.1°), and O−Al−O bond angle (89.9°) in **7b** compare to $[(Ar^{Me,H}O)_2(THF)_2Yb^{III}(\mu\text{-}OAr^{Me,H})_2AlMe_2]$ (1.846(10) Å/65.6(9)°/85.1(6)°).[54] The Yb−O−C_{ipso} angles (av 131.6°) lie in the range of those found for the bridging aryloxide ligands in $Y^{III}(OAr^{iPr,H})[(\mu\text{-}OAr^{iPr,H})(\mu\text{-}Me)AlMe_2]_2$ (125.33(9)° and 129.0(1)°)[17] and $Sm^{III}(OAr^{iPr,H})[(\mu\text{-}OAr^{iPr,H})(\mu\text{-}Me)AlMe_2]_2$ (125.9(3)° and 135.2(2)°).[15]

$[Ln(AlEt_4)_2]_n$−$HOAr^{iPr,H}$ Reactions. Similar to the $[Yb(AlMe_4)_2]_n$−$HOAr^{iPr,H}$ reaction, treatment of hexane-soluble $[Sm(AlEt_4)_2]_n$ (**2a**) with 2 equiv of $HOAr^{iPr,H}$ gave predominantly ligand redistribution yielding dark-red $Sm[(\mu\text{-}OAr^{iPr,H})_2(AlEt_2)]_2$ (**8a**) as the main product. Complex **8a** exhibits a coordination environment and geometry similar to that found in **7b** (Figure 5, Table 4). As discussed for **7b**, a close contact between the metal center and one of the *i*Pr-groups (Sm···C16 = 3.186 Å) suggests steric saturation by agostic interactions also in **8a**. The average Sm−O bond distance of 2.484 Å agrees with those in $[(C_5Me_5)Sm(\mu\text{-}OC_6H_2tBu_3\text{-}2,4,6)]_2$ (Table 2).[30]

The analogous reaction between $[Yb(AlEt_4)_2]_n$ (**2b**) and $HOAr^{iPr,H}$ (2 equiv, 16 h, ambient temperature) resulted in a product mixture, which after crystallization from hexane at −35 °C yielded at least two crystalline compounds as indicated by their different crystal morphologies. Fractionate crystallization and X-ray diffraction studies revealed the formation of an ytterbium dimer of the composition $[Et_2Al(\mu\text{-}OAr^{iPr,H})_2Yb(\mu\text{-}Et)_2AlEt(\mu\text{-}Et)]_2$ (**9**) and monomeric bis(TEA)mono(THF) adduct $Yb[(\mu\text{-}OAr^{iPr,H})(\mu\text{-}Et)AlEt_2]_2(THF)$ (**10**) (Figures 6 and 7, Tables 5 and 6). While compound **9** was identified as the main product by NMR spectroscopy, adventitious amounts of THF facilitated the crystallization of complex **10** as a minor coproduct. Complex **9** once more proves that $[R_2Al(\mu\text{-}OAr^{iPr,H})]$-promoted ligand rearrangement is a favorable reaction pathway at large Ln^{II} centers. Moreover, complex **9** features the only isolated complex in this study with intact tetraalkylaluminate ligands (coordination mode = $\mu_2\text{-}\eta^2\text{:}\eta^1$).[55]

The ytterbium centers in **9** feature a distorted square pyramidal coordination geometry with two aryloxide oxygen atoms of the rearranged bidentate ligand $[Et_2Al(\mu\text{-}OAr^{iPr,H})_2]$ ligand and two methylene carbon atoms of the η^2-coordinated tetraethylaluminate ligand in the basal positions. The apical position is occupied by the methylene carbon atom of the second η^1-coordinated tetraethylaluminate ligand. In complex **10**, the ligands also adopt a square pyramidal geometry, with one THF molecule in the apical position and two $[(\mu\text{-}OAr^{iPr,H})(\mu\text{-}Et)AlEt_2]$ units forming the basal plane. The Yb−C bond distances average 2.678 Å (**9**) and 2.678 Å (**10**) and are comparable to those in $Yb(AlEt_4)_2(THF)_2$ (av 2.663 Å)[26] and $[Yb(AlEt_4)_2]_n$ (**2b**, av 2.675 Å).[56] These bridging Yb−C bond distances, however, are markedly longer than the Yb−C σ-bonds in $Yb[C(SiMe_3)_2(SiMe_2CH{=}CH_2)]I(OEt_2)$ (2.50(2) Å),[57] and $Yb(C_6H_3Ph_2\text{-}2,6)I(THF)_3$ (2.529(4) Å).[58] The average Yb−O bond distances in **9** (2.337 Å) and **10** (2.318 Å) lie in the range of Yb−(μ-OAr) distances (Table 2); however, they are shorter than in **7b** (2.383 Å).

An interesting aspect of the molecular structures of **9** and **10** is the coordination mode of the bridging ethyl groups. All the relevant hydrogen atoms were located in the difference Fourier maps and refined isotropically. Because

(53) Troyanov, S. I. *Russ. J. Coord. Chem.* **1998**, *24*, 351.
(54) Evans, W. J.; Ansari, M. A.; Ziller, J. W. *Inorg. Chem.* **1995**, *34*, 3079.
(55) Dietrich, H. M.; Schuster, O.; Törnroos, K. W.; Anwander, R. *Angew. Chem., Int. Ed.* **2006**, *45*, 4858.
(56) Klimpel, M. G.; Anwander, R.; Tafipolsky, M.; Scherer, W. *Organometallics* **2001**, *20*, 3983.
(57) Eaborn, C.; Hitchcock, P. B.; Izod, K.; Lu, Z. R.; Smith, J. D. *Organometallics* **1996**, *15*, 4783.

Table 4. Selected Bond Distances (Å) and Angles (deg) for Complexes **7b** and **8a**

bond distances	7b	8a	bond distances	7b	8a
Ln···Al1	3.2916(10)	3.4162(14)	O2−C15[b]	1.386(3)	1.384(5)
Ln···Al2	3.3056(9)	3.3381(14)	O3−C29[c]	1.389(3)	1.383(5)
Ln−O1	2.364(2)	2.457(3)	O4−C41[d]	1.387(3)	1.389(6)
Ln−O2	2.407(2)	2.517(2)	Al1−C1	1.958(4)	1.968(6)
Ln−O3	2.365(2)	2.451(3)	Al1−C2[e]	1.950(4)	1.946(5)
Ln−O4	2.399(2)	2.531(3)	Al2−C27[f]	1.966(4)	1.952(7)
Al1−O1	1.849(2)	1.842(4)	Al2−C28[g]	1.964(3)	1.967(6)
Al1−O2	1.829(2)	1.838(3)	Ln···C13[h]	3.055(4)	3.186(7)
Al2−O3	1.840(2)	1.824(4)	Ln···C36	3.067(4)	
Al2−O4	1.839(2)	1.839(4)	Ln···H13A[h]	2.56(3)	2.62
O1−C3[a]	1.390(4)	1.372(5)	Ln···H36B	2.52(3)	
bond angles	**7b**	**8a**	**bond angles**	**7b**	**8a**
O1−Ln−O2	66.36(7)	62.90(10)	Ln−O1−C3[a]	133.84(2)	127.5(2)
O3−Ln−O4	65.84(7)	61.67(10)	Ln−O2−C15[b]	132.82(17)	130.3(3)
O1−Al1−O2	90.46(10)	89.72(14)	Ln−O3−C29[c]	129.22(18)	137.2(3)
O3−Al2−O4	89.47(10)	88.43(15)	Ln−O4−C41[d]	130.67(16)	134.8(3)

[a] C5. [b] C17. [c] C33. [d] C45. [e] C3. [f] C29. [g] C31. [h] C16 in complex **8a**.

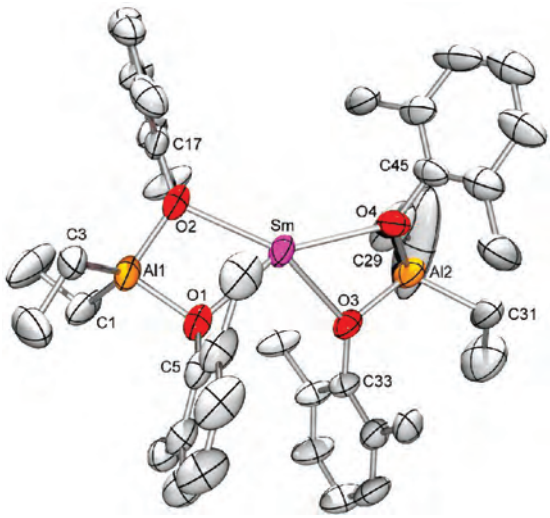

Figure 5. Molecular structure of **8a**. Atomic displacement parameters are set at the 50% probability level, and hydrogen atoms and *i*Pr-methyl groups are omitted for clarity.

of the steric unsaturation of the metal center in **9**, both of the hydrogen atoms in the bridging CH_2 groups, and additionally one hydrogen atom of the CH_3 group in the μ,η^1-coordinated $[AlEt_4]^-$ moiety are directed toward the Yb atom (Yb···C6 = 2.9694(17) Å, Figure 6B). In complex **10**, both hydrogen atoms on C13, together with H31A and H32B, are positioned near the Yb center, suggesting one Yb···H−C β-agostic and three Yb···H−C α-agostic interactions. A similar structural motif was detected in the Sm^{III} bis(TEA) adduct complex $Sm(OAr^{iPr,H})[(\mu\text{-}OAr^{iPr,H})(\mu\text{-}Et)AlEt_2]_2$.[16] While the $Ln-C_{CH_2}-C_{CH_3}$ bond angles in the latter complex are almost linear (av 166.3(5)°),[16] the C5−C6 (**9**) and C31−C32 (**10**) ethyl groups approach the Yb center side-on forming short $Yb\cdots C_{CH_3}$ interactions (2.9694(17) and 3.020(3) Å for **9** and **10**, respectively). As a consequence, the $Yb-C_{CH_2}-C_{CH_3}$ angles are 82.11(9)° (**9**) and 88.02(18)° (**10**), corroborating agostic deformations.[56,59,60] Similar side-on bondings of ethyl groups were previously found in $(C_5Me_5)_2Yb(\mu\text{-}Et)(AlEt_2)(THF)$ ($Yb\cdots C_{CH_3}$ = 2.939(21) Å, Yb−C−C = 76.6°),[61] $[Yb(AlEt_4)_2]_n$ (**2b**, $Yb\cdots C_{CH_3}$ = 3.056(9)−3.364(6) Å, Yb−C−C = 85.3(4)−97.3(3)°),[56] and $[Sm(AlEt_4)_2]_n$ (**2a**, av $Sm\cdots C_{CH_3}$ = 3.215 Å, Sm−C−C = 82.7(6)−93.0(5)°).[22]

Conclusions

Peralkylated complexes $[Ln(AlR_4)_2]_n$ readily undergo protonolysis/alkane elimination reactions with bulky phenolic substrates $HOAr^{tBu,Me}$ and $HOAr^{iPr,H}$. Two prevalent secondary reaction pathways have been unambiguously identified, TMA(TEA) adduct formation and ligand rearrangement under formation of the new bidentate ligands $[(\mu\text{-}OAr^{iPr,H})_2AlMe_2]$ and $[(\mu\text{-}OAr^{iPr,H})_2AlEt_2]$. These are known reaction patterns from trivalent organo-rare-earth metal chemistry involving binary mixtures $Ln(OAr)_3(THF)_x/AlR_3$ with smaller methyl-substituted phenol ligands (see Chart 1, **C** and **D**). Although, the larger Ln^{II} metal centers can template the formation of $[(\mu\text{-}OAr^{iPr,H})_2AlEt_2]$ moieties, the *tert*-butyl-substituted aryloxides seem to be too bulky to engage in such a ligand rearrangement. Because of the absence of donor solvent molecules the new homo- and heteroleptic aryloxide complexes are stereoelectronically unsaturated and, hence, feature distinct secondary intramolecular interactions comprising close $Ln-C_{ipso}$(aryloxide) and $Ln-\pi_{arene}$(solvent) contacts, as well as $Ln^{II}\cdots(H-C)$ α- and β-agostic interactions with bridging methyl/ethyl ligands and the *i*Pr groups of $[OAr^{iPr,H}]$.

Experimental Section

General Considerations. All manipulations were performed under an argon atmosphere with rigorous exclusion of oxygen and water, using standard Schlenk, high-vacuum, and glovebox techniques (MBraun MB150B-G-II; <1 ppm O_2, <1 ppm H_2O). Hexane, toluene, and THF were purified using Grubbs columns (MBraun SPS, solvent purification system). C_6D_6 was obtained from Aldrich, dried over Na for 24 h, filtered, and stored in the glovebox. Trimethyl-, and triethylaluminum, and 2,6-di-isopropylphenol were purchased from Aldrich and used as received. 2,6-Di-*tert*-butyl-4-methylphenol (Aldrich) was sublimed prior to use. Complexes $[Ln(AlR_4)_2]_n$ (R = Me

(58) Heckmann, G.; Niemeyer, M. *J. Am. Chem. Soc.* **2000**, *122*, 4227.
(59) Burger, B. J.; Thompson, M. E.; Cotter, W. D.; Bercaw, J. E. *J. Am. Chem. Soc.* **1990**, *112*, 1566.
(60) Haaland, A.; Scherer, W.; Ruud, K.; McGrady, G. S.; Downs, A. J.; Swang, O. *J. Am. Chem. Soc.* **1998**, *120*, 3762.
(61) Yamamoto, H.; Yasuda, H.; Yokota, K.; Nakamura, A.; Kai, Y.; Kasai, N. *Chem. Lett.* **1988**, 1963.

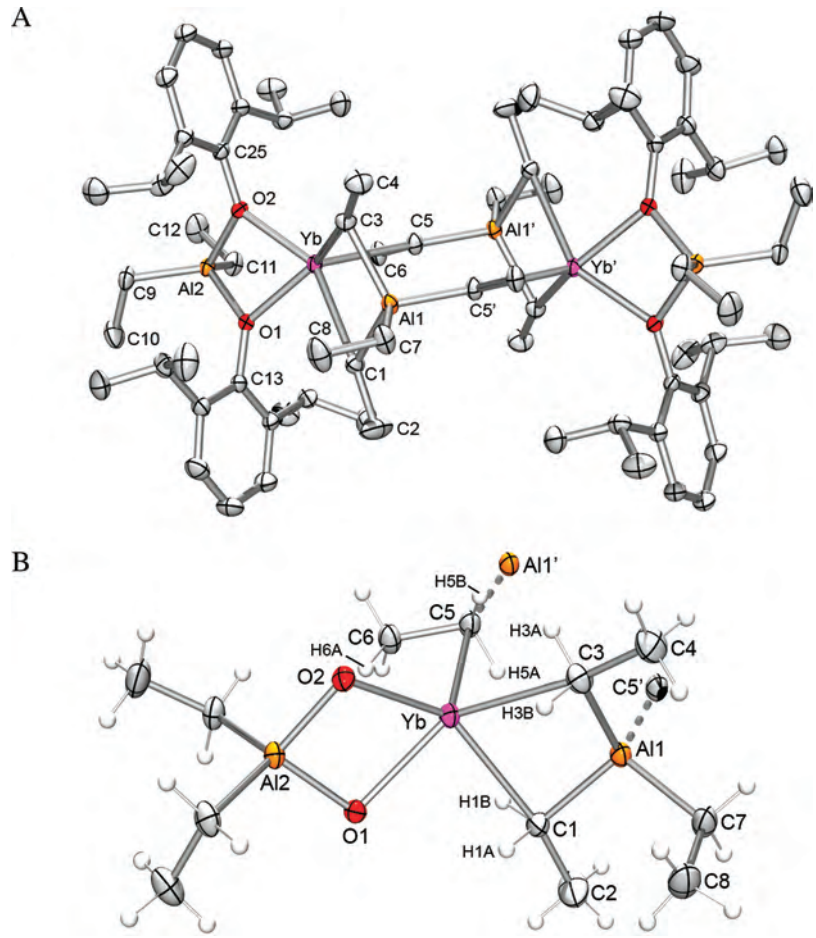

Figure 6. (A) Molecular structure of **9** with atomic displacement parameters set at the 50% probability level; hydrogen atoms are omitted for clarity. (B) Yb^{II} coordination environment in **9** emphasizing the agostically interacting hydrogen atoms (atomic displacement parameters set at the 50% probability level).

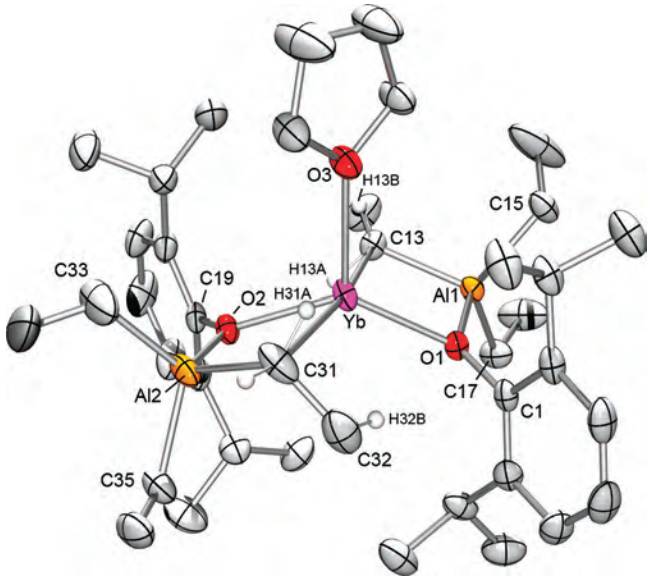

Figure 7. Molecular structure of **10** with atomic displacement parameters set at the 50% probability level. Hydrogen atoms are omitted for clarity, except for agostically interacting H13A/B, H31A, and H32B.

(**1**), Et (**2**)) were synthesized according to literature procedures.[22,56] NMR spectra were recorded at 298 K on a Bruker-AV600 (5 mm cryo probe, ^{1}H 600.13 MHz; ^{13}C 150.91 MHz). ^{1}H and ^{13}C shifts are referenced to internal solvent resonances and reported in parts per million relative to TMS. IR spectra were recorded on a Nicolet-Impact 410 FTIR spectrometer as Nujol mulls sandwiched between CsI plates. Elemental analyses were performed on an Elementar Vario EL III. Crystallographic data for complexes **5**, **6**, **7b**, **8a**, **9**, and **10** are compiled in Table 7.

Table 5. Selected Bond Distances (Å) and Angles (deg) for Complex **9**

	bond distances		
Yb···Al1	3.1408(4)	Al1−C7	1.9785(17)
Yb···Al2	3.2339(4)	Al2−C9	1.9666(16)
Yb−O1	2.3268(10)	Al2−C11	1.9798(17)
Yb−O2	2.3473(10)	O1−C13	1.3875(17)
Yb−C1	2.6511(15)	O2−C25	1.3944(17)
Yb−C3	2.6202(16)	Yb···H1A	2.494(2)
Yb−C5	2.7626(16)	Yb···H1B	2.42(2)
Yb···C6	2.9694(17)	Yb···H3A	2.44(2)
Al1−O1	1.8323(11)	Yb···H3B	2.42(2)
Al2−O2	1.8463(11)	Yb···H5A	2.54(2)
Al1−C1	2.0392(16)	Yb···H5B	2.52(2)
Al1−C3	2.0634(17)	Yb···H6A	2.42(2)
Al1−C5	2.0321(16)		
	bond angles		
O1−Yb−O2	66.30(3)	Yb−O2−C25	131.49(8)
C1−Yb−C3	79.10(5)	Yb−C1−C2	168.52(13)
O1−Yb−C3	140.47(4)	Yb−C3−C4	169.32(12)
O2−Yb−C1	149.90(4)	Yb−C5−C6	82.11(9)
Yb−O1−C13	126.90(8)		

General Procedure for the Synthesis of Ln[(μ-OAr$^{t\mathrm{Bu,Me}}$)-(μ-Me)AlMe$_2$]$_2$ (3). To a suspension of [Ln(AlMe$_4$)$_2$]$_n$ (**1**) in toluene, a solution of HOAr$^{t\mathrm{Bu,Me}}$ diluted in toluene was slowly added. Gas formation and color changes were observed (Ln = Sm, dark purple to reddish brown; Ln = Yb, pale yellow to bright

Table 6. Selected Bond Distances (Å) and Angles (deg) for **10**

bond distances			
Yb···Al1	3.3142(7)	Al1−C13	2.035(3)
Yb···Al2	3.2032(8)	Al1−C15	1.987(3)
Yb−O1	2.3303(17)	Al1−C17	1.981(3)
Yb−O2	2.3057(17)	Al2−C31	2.049(3)
Yb−O3	2.3873(19)	Al2−C33	1.969(4)
Yb−C13	2.700(2)	Al2−C35	1.980(3)
Yb−C31	2.656(3)	Yb···H13A	2.41(3)
Al1−O1	1.8603(18)	Yb···H13B	2.45(3)
Al2−O2	1.8524(2)	Yb···H31A	2.38(4)
O1−C1	1.388(3)	Yb···C32	3.020(3)
O2−C19	1.381(3)	Yb···H32B	2.48(4)
bond angles			
O1−Yb−O2	128.87(6)	Yb−O1−C1	126.16(14)
C13−Yb−C31	164.63(9)	Yb−O2−C19	130.17(14)
O1−Yb−C13	69.94(7)	Yb−C13−C14	161.5(2)
O2−Yb−C31	74.21(8)	Yb−C31−C32	88.02(18)

Table 7. Crystallographic Data for Complexes **5**, **6**, **7b**, **8a**, **9**, and **10**

	5	**6**	**7b**
chemical formula	$C_{73}H_{118}Al_2O_4Sm_2$	$C_{52}H_{82}Al_2O_3Sm$	$C_{52}H_{80}Al_2O_4Y$
M_r	1414.33	959.49	996.16
space group	$P\bar{1}$	$P\bar{1}$	$P\bar{3}1c$
a (Å)	12.9908(4)	11.7050(4)	20.9364(3)
b (Å)	13.9942(4)	13.5958(5)	20.9364(3)
c (Å)	20(8444(7)	18.0156(7)	43.7686(13)
α (deg)	78.114(1)	72.128(1)	90
β (deg)	76.426(1)	80.171(1)	90
γ (deg)	77.902(1)	67.093(1)	120
V (Å^3)	3552.43(19)	2509.15(16)	16614.9(6)
Z	2	2	12
F(000)	1476	1012	6240
T (K)	123(2)	123(2)	123(2)
ρ_{calcd} (g cm^{-3})	1.322	1.270	1.195
μ (mm^{-1})	1.706	1.244	1.758
R1[a] (obsd), wR2[b] (all)	0.0252, 0.0579	0.0365, 0.0965	0.0458, 0.0867
S[c]	1.044	1.075	1.221
	8a	**9**	**10**
chemical formula	$C_{56}H_{88}Al_2O_4Sm$	$C_{36}H_{64}Al_2O_2Yb$	$C_{40}H_{72}Al_2O_3Yb$
M_r	1029.57	755.87	827.98
space group	$P2_12_12_1$	$Pbca$	$P2_1/c$
a (Å)	16.2302(6)	18.7310(7)	18.3390(6)
b (Å)	18.4725(7)	20.1036(7)	12.8562(4)
c (Å)	18.7583(7)	20.4087(7)	19.6956(6)
α (deg)	90	90	90
β (deg)	90	90	114.234(1)
γ (deg)	90	90	90
V (Å^3)	5624.0(4)	7685.1(5)	4234.4(2)
Z	4	8	4
F(000)	2176	3136	1728
T (K)	123(2)	123(2)	123(2)
ρ_{calcd} (g cm^{-3})	1.216	1.307	1.299
μ (mm^{-1})	1.116	2.506	2.282
R1[a] (obsd), wR2[b] (all)	0.0370, 0.0994	0.0192, 0.0446	0.0309, 0.0781
S[c]	1.088	1.078	1.119

[a] $R1 = \sum(|F_o| - |F_c|)/\sum|F_o|$. [b] $wR2 = \{\sum[w(F_o^2 - F_c^2)^2]/\sum[w(F_o^2)^2]\}^{1/2}$. [c] $S = [\sum w(F_o^2 - F_c^2)^2/(n_o - n_p)]^{1/2}$.

yellow). After it had been stirred overnight, the suspension was centrifuged and filtered, and the volume was reduced. Crystallization was performed in toluene at –35 °C.

Sm[(μ-OAr^{tBu,Me})(μ-Me)AlMe$_2$]$_2$ (3a). Following the procedure described above, [Sm(AlMe$_4$)$_2$]$_n$ (**1a**, 0.053 g, 0.16 mmol) and HOAr^{tBu,Me} (0.058 g, 0.32 mmol) yielded **3a** as a reddish brown solid (0.103 g, 0.14 mmol, 45%). IR (Nujol, cm^{-1}): 1600 w, 1422 s, 1365 s, 1296 w, 1261 m, 1237 m, 1227 m, 1201 s, 1154 w, 1124 w, 1019 m, 953 w, 889 m, 860 m, 833 m, 806 w, 774 m, 721 s, 699 s, 674 w, 576 w, 539 w. ^{1}H NMR (C$_6$D$_6$, 25 °C): δ 7.97 (s, 4H, Ar*H*), 3.49 (s, 36H, C*Me$_3$*), 2.77 (s, 6H, Ar*Me*), –20.99 (s, 18H, (μ-*Me*)Al*Me$_2$*). ^{13}C NMR (C$_6$D$_6$, 25 °C): δ 132.0, 129.7, 125.2 (Ar*C*), 49.3 (*C*Me$_3$), 42.3 (C*Me$_3$*), 21.8 (Ar*Me*), –13.6 ((μ-*Me*)Al*Me$_2$*). Anal. Calcd for C$_{36}$H$_{64}$Al$_2$O$_2$Sm (733.2 g mol^{-1}): C 58.97, H 8.80. Found: C 57.68, H 8.35.

Yb[(μ-OAr^{tBu,Me})(μ-Me)AlMe$_2$]$_2$ (3b). Following the procedure described above, [Yb(AlMe$_4$)$_2$]$_n$ (**1b**, 0.047 g, 0.14 mmol) and HOAr^{tBu,Me} (0.061 g, 0.28 mmol) yielded **3b** as a yellow solid (0.070 g, 0.09 mmol, 68%). IR (Nujol, cm^{-1}): 1412 m, 1266 w, 1255 w, 1230 m, 1216 w, 1205 m, 1191 m, 1171 w, 863 w, 830 w, 818 w, 805 w, 774 w, 695 m, 600 m, 529 w. ^{1}H NMR (C$_6$D$_6$, 25 °C): δ 7.00 (s, 4H, Ar*H*), 2.11 (s, 6H, Ar*Me*), 1.32 (s, 36H, C*Me$_3$*), –0.10 (s, 18H, (μ-*Me*)Al*Me$_2$*). ^{13}C NMR (C$_6$D$_6$, 25 °C): δ 151.5 (*C*$_{ipso}$), 139.7, 129.8, 125.4 (Ar*C*), 35.3 (*C*Me$_3$), 32.3 (C*Me$_3$*), 20.9 (Ar*Me*), –0.8 ((μ-*Me*)Al*Me$_2$*). Anal. Calcd for C$_{36}$H$_{64}$Al$_2$O$_2$Yb (755.9 g mol^{-1}): C 57.20, H 8.53. Found: C 57.63, H 8.66.

General Procedure for the Synthesis of Ln[(μ-OAr^{tBu,Me})-(μ-Et)AlEt$_2$]$_2$ (4). To a solution of [Ln(AlEt$_4$)$_2$]$_n$ (**2**) in hexane, a solution of HOAr^{tBu,Me} diluted in hexane was slowly added. Gas formation and color change were observed (Ln = Sm, dark purple to reddish brown; Ln = Yb, pale yellow to bright yellow). After it had been stirred overnight, the solution was filtered, and the volume was reduced. Crystallization was performed in hexane at −35 °C.

Sm[(μ-OAr^{tBu,Me})(μ-Et)AlEt$_2$]$_2$ (4a). Following the procedure described above, [Sm(AlEt$_4$)$_2$]$_n$ (**2a**, 0.047 g, 0.11 mmol) and HOAr^{tBu,Me} (0.048 g, 0.22 mmol) yielded **4a** as a brown solid (0.079 g, 0.14 mmol, 89%). ^{1}H NMR (C$_6$D$_6$, 25 °C): δ 7.08 (s, 4H, Ar*H*), 3.68 (s, 36H, C*Me$_3$*), 1.97 (s, 6H, Ar*Me*), –0.73 (s, 18H, (μ-CH$_2$C*H$_3$*)Al(CH$_2$C*H$_3$*)$_2$), –16.95 (s, 12H, (μ-C*H$_2$*CH$_3$)Al(C*H$_2$*CH$_3$)$_2$). ^{13}C NMR (C$_6$D$_6$, 25 °C): δ 132.0 (Ar*C*), 129.7 (Ar*C*), 125.2 (Ar*C*), 121.5 (Ar*C*), 49.3 (*C*Me$_3$), 42.3 (C*Me$_3$*), 21.8 (Ar*Me*), –13.7 ([μ-*Et*]Al*Et$_2$*). Anal. Calcd for C$_{42}$H$_{76}$Al$_2$O$_2$Sm (817.4 g mol^{-1}): C 61.72, H 9.37. Found: C 60.13, H 8.7.

Yb[(μ-OAr^{tBu,Me})(μ-Et)AlEt$_2$]$_2$ (4b). Following the procedure described above, [Yb(AlEt$_4$)$_2$]$_n$ (**2b**, 0.057 g, 0.12 mmol) and HOAr^{tBu,Me} (0.055 g, 0.25 mmol) yielded **4b** as a yellow solid (0.097 g, 0.12 mmol, 94%). IR (Nujol, cm^{-1}): 1294 w, 1262 s, 1205 w, 1120 w, 1093 m, 1052 m, 918 w, 890 m, 860 m, 843 w, 805 w, 774 w, 722 m, 640 s, 540 w. ^{1}H NMR (C$_6$D$_6$, 25 °C): δ 7.01 (s, 4H, Ar*H*), 2.10 (s, 6H, Ar*Me*), 1.38 (t, $^3J_{H,H}$ = 7.9 Hz, 18H, (μ-CH$_2$C*H$_3$*)Al(CH$_2$C*H$_3$*)$_2$), 1.34 (s, 36H, C*Me$_3$*), 0.38 (q, $^3J_{H,H}$ = 7.8 Hz, 12H, ((μ-C*H$_2$*CH$_3$)Al(C*H$_2$*CH$_3$)$_2$). ^{13}C NMR (C$_6$D$_6$, 25 °C): δ 152.3 (*C*$_{ipso}$), 139.4 (*C*$_{orto}$), 129.7 (*C*$_{para}$), 125.7 (*C*$_{meta}$), 35.6 (*C*Me$_3$), 32.5 (C*Me$_3$*), 20.8 (Ar*Me*), 10.9 ((μ-CH$_2$*C*H$_3$)Al(CH$_2$*C*H$_3$)$_2$), 7.2 ((μ-*C*H$_2$CH$_3$)Al(*C*H$_2$CH$_3$)$_2$). Anal. Calcd for C$_{42}$H$_{76}$Al$_2$O$_2$Yb (840.1 g mol^{-1}): C 60.05, H 9.12. Found: C 60.83, H 9.27.

General Procedure for the Synthesis of Ln[(μ-OAr^{iPr,H})$_2$-AlMe$_2$]$_2$ (7). [Ln(AlMe$_4$)$_2$]$_n$ (**1**) was suspended in toluene, and a solution of HOAr^{iPr,H} diluted in toluene was slowly added. Gas evolution and color change were observed (Ln = Sm, dark purple to dark red; Ln = Yb, pale yellow to red). The mixture was stirred for 16 h at ambient temperature, filtered to remove insoluble parts, dried in vacuo, and finally crystallized from hexane at −35 °C.

[Sm(μ-OAr^{iPr,H})$_x$AlMe$_y$] (7a). Following the procedure described above, [Sm(AlMe$_4$)$_2$]$_n$ (**1a**, 0.044 g, 0.14 mmol) and HOAr^{iPr,H} (0.051 g, 0.29 mmol) yielded a reddish brown solid (0.041 g, 0.04 mmol, 58%). Possible product Sm[(μ-OAr^{iPr,H})$_2$AlMe$_2$]$_2$ (**7a**). IR (Nujol, cm^{-1}): 1590 m, 1339 m, 1325 m, 1259 m, 1200 m, 1173 m, 1099 m, 1055 w, 1042 m, 934 w, 920 w, 888 m, 865 w, 834 s, 799 m, 756 s, 722 m, 691 s, 677 m, 620 w, 573 w. ^{1}H NMR (C$_6$D$_6$, 25 °C): δ 5.34, 5.09, 1.44–0.86, –9.55. ^{13}C NMR (C$_6$D$_6$, 25 °C): δ

165.7, 120.1, 119.1, 118.0, 55.6, 30.0, –24.8. Anal. Calcd for $C_{52}H_{80}Al_2O_4Sm$ (973.5 g mol^{-1}): C 64.15, H 8.28. Found: C 63.42, H 7.80.

Yb[(μ-OAr^{iPr,H})$_2$AlMe$_2$]$_2$ (7b). Following the procedure described above, $[Yb(AlMe_4)_2]_n$ (**1b**, 0.044 g, 0.13 mmol) and HOAr^{iPr,H} (0.048 g, 0.27 mmol) yielded **7b** as yellow crystals (0.058 g, 0.06 mmol, 86%). IR (Nujol, cm^{-1}): 1590 m, 1339 s, 1260 s, 1244 m, 1200 m, 1174 s, 1160 m, 1100 m, 1056 w, 1043 m, 934 m, 920 w, 889 w, 833 s, 799 m, 756 s, 722 m, 691 s, 670 m, 617 m, 578 m. ^{1}H NMR (C_6D_6, 25 °C): δ 7.01–6.91 (m, 12H Ar*H*), 3.60 (sept, 8H, C*H*Me$_2$), 1.09 (d, 48H, CH*Me$_2$*), –0.62 (s, 12H, Al(C*H*$_3$)$_2$). ^{13}C NMR (C_6D_6, 25 °C): δ 149.2 (C_{ipso}), 138.3 (C_{ortho}), 124.4 (C_{meta}), 123.0 (C_{para}), 26.6 (*C*HMe$_2$), 24.6 (CH*Me$_2$*), –8.2 (Al*Me$_2$*). Anal. Calcd for $C_{52}H_{80}Al_2O_4Yb$ (996.2 g mol^{-1}): C 62.69, H 8.09. Found: C 63.81, H 8.06.

Sm[(μ-OAr^{iPr,H})$_2$AlEt$_2$]$_2$ (8a). To a stirred solution of $[Sm(AlEt_4)_2]_n$ (**2a**, 0.170 g, 0.39 mmol) in hexane a solution of HOAr^{iPr,H} (0.142 g, 0.80 mmol) diluted in hexane was slowly added. Gas formation and a color change of the reaction mixture from dark purple to reddish brown were observed. After it had been stirred overnight, the solution was filtered, and the volume reduced. Dark-red crystals of **8a** (0.128 g, 0.12 mmol, 62%) were grown from hexane at −35 °C. IR (Nujol, cm^{-1}): 1590 m 1341 s, 1260 s, 1203 m, 1172 m, 1100 m, 1044 m, 935 w, 920 w, 888 m, 861w, 833 s, 798 m, 756 s, 723 s, 690 m, 641 m. ^{1}H NMR (C_6D_6, 25 °C): δ 5.37, 5.12, –5.19, –8.68. ^{13}C NMR (C_6D_6, 25 °C): δ 163.8 (C_{ipso}), 137.0, 120.1, 117.9 (Ar*C*), 55.1, 23.7, –16.2. Anal. Calcd for $C_{56}H_{88}Al_2O_4Sm$ (1029.6 g mol^{-1}): C 65.33, H 8.61. Satisfactory microanalytical data could not be obtained.

[Et$_2$Al(μ-OAr^{iPr,H})$_2$Yb(μ-Et)$_2$AlEt(μ-Et)]$_2$ (9). To a stirred solution of $[Yb(AlEt_4)_2]_n$ (**2b**, 0.091 g, 0.20 mmol) in hexane a solution of HOAr^{iPr,H} (0.071 g, 0.40 mmol) diluted in hexane was slowly added. Gas formation and color change of the reaction mixture from yellow to orange were observed. After it had been stirred overnight, the solution was filtered, and the volume was reduced. Fractionate crystallization at −35 °C yielded **9** and **10** as yellow crystals. Because there are several products in the reaction mixture, the NMR spectra could not be unambiguously assigned and satisfactory microanalytical data could not be obtained. Tentatively, the following assignment is made for **9**. ^{1}H NMR (C_6D_6, 25 °C): δ = 6.98 (s, 4H Ar*H*), 6.95–6.90 (m, 8H Ar*H*), 3.65 (sept, 8H, C*H*Me$_2$), 1.22 (s, br, 48H, CH*Me$_2$*), 1.16 (t, $^3J_{H,H}$ = 7.8 Hz, 24H, Al(CH$_2$C*H*$_3$)$_4$), 1.06 (t, $^3J_{H,H}$ = 8.4 Hz, 12H, Al(CH$_2$C*H*$_3$)$_2$), 0.20 (q, $^3J_{H,H}$ = 8.4 Hz, 8H, Al(C*H*$_2$CH$_3$)$_2$), 0.18 (q, $^3J_{H,H}$ = 7.8 Hz, 16H, Al(C*H*$_2$CH$_3$)$_4$).

Acknowledgment. We are grateful to the Norwegian Research Council (Project No. 182547/I30) and the program Nanoscience@UiB for generous financial support.

Supporting Information Available: ^{1}H NMR spectrum of $[Yb(AlEt_4)_2]_n$ (**2b**) contaminated with $Yb(AlEt_4)_2(THF)_2$ and full crystallographic data for complexes **5**, **6**, **7b**, **8a**, **9**, and **10**. This material is available free of charge *via* the Internet at http://pubs.acs.org.

IC702517S